A Scheme for Calculation of the Liquid Fraction in Mixed-Phase Stratiform Clouds in Large-Scale Models

LEON D. ROTSTAYN, BRIAN F. RYAN, AND JACK J. KATZFEY

CSIRO Atmospheric Research, Aspendale, Victoria, Australia

(Manuscript received 28 August 1998, in final form 26 March 1999)

ABSTRACT

A scheme for calculation of the liquid fraction f_l in mixed-phase stratiform clouds has been developed for use in large-scale models. An advantage of the scheme, compared to the interpolation in temperature that is typically used, is that it makes it possible to simulate the life cycles of mixed-phase clouds, and the differences between deep and shallow clouds. The central part of the scheme is a physically based calculation of the growth of cloud ice crystals by vapor deposition at the expense of coexisting cloud liquid water, the so-called Bergeron–Findeisen mechanism. Versions of this calculation have been derived for three different ice-crystal habits (spheres, hexagonal plates, or columns) and for two different assumed spatial relationships of the coexisting cloud ice and liquid water (horizontally adjacent or uniformly mixed). The scheme also requires a parameterization of the ice crystal number concentration N_i.

The variation with temperature of f_l looks broadly realistic compared to aircraft observations taken in the vicinity of the British Isles when the scheme is used in the CSIRO GCM, if N_i is parameterized using a supersaturation-dependent expression due to Meyers et al. If Fletcher's earlier temperature-dependent expression for N_i is used, the scheme generates liquid fractions that are too large. There is also considerable sensitivity to the ice-crystal habit, and some sensitivity to model horizontal resolution and to the assumed spatial relationship of the liquid water and ice. A further test shows that the liquid fractions are lower in cloud layers that are seeded from above by falling ice, than in layers that are not seeded in this way.

The scheme has also been tested in limited-area model simulations of a frontal system over southeastern Australia. Supercooled liquid water forms initially in the updraft, but mature parts of the cloud are mostly glaciated down to the melting level. This behavior, which is considered to be realistic based on observations of similar cloud systems, is not captured by a conventional temperature-dependent parameterization of f_l. The variation with temperature of f_l shows a marked sensitivity to the assumed spatial relationship of the liquid water and ice. The results obtained using the uniformly mixed assumption are considered to be more realistic than those obtained using the horizontally adjacent assumption. There is also much less sensitivity to the time step when the former assumption is used.

1. Introduction

The treatment of mixed-phase clouds in global climate models (GCMs) and other large-scale atmospheric models is quite crude at present. The coexistence of cloud liquid water and cloud ice adds considerably to the complexity of the microphysical processes that must be modeled (e.g., Ryan 1996), but these are greatly oversimplified even in state-of-the-art cloud schemes.

Of particular interest is the parameterization of the fraction of condensate that exists as supercooled liquid water in mixed-phase clouds, hereafter referred to as the liquid fraction. The radiative properties of cloud ice and cloud liquid water are very different, with ice generally having a much larger effective radius and, hence, a much smaller optical depth for a given cloud water path. Their microphysical properties are also very different, with ice crystals tending to grow rapidly to precipitable size, especially in the presence of supercooled liquid water. This is the rationale behind the seeding of supercooled clouds with efficient ice nuclei such as silver iodide. In a time-averaged sense, the microphysical and radiative differences between ice and liquid water act in the same direction, because inclusion of efficient frozen precipitation processes in a model will tend to reduce the cloud water path, thereby reinforcing the purely radiative effect of smaller optical depth for a given cloud water path. Another reason why accurate parameterization of the liquid fraction may be important is that the release of latent heat of fusion can affect cloud dynamics and hence cloud depth and microphysics (Raymond and Blyth 1992).

Some previous authors have shown that the treatment of the liquid fraction in global models can affect either their climate sensitivity or their mean climate. Li and

Corresponding author address: Leon D. Rotstayn, CSIRO, Private Mail Bag 1, Aspendale, Victoria 3195, Australia.
E-mail: Leon.Rotstayn@dar.csiro.au

Le Treut (1992) found that the response of their GCM to an imposed warming was sensitive to the threshold temperature below which clouds were assumed to be composed of ice rather than liquid water. Gregory and Morris (1996) found that both the control climate and the response to a doubling of CO_2 were somewhat sensitive to the parameterization of the liquid fraction in mixed-phase clouds in the U.K. Meteorological Office (UKMO) Unified Model.

Many existing cloud schemes use some form of interpolation in temperature to specify the liquid fraction at temperatures below freezing (Smith 1990; Ose 1993; Kristjánsson 1994; Boucher et al. 1995; Fowler et al. 1996; Rasch and Kristjánsson 1998). The lower temperature limit, at which all condensate is assumed to form as ice, differs strongly among these models. For example, Smith (1990) and Boucher et al. (1995) assumed a lower limit of $-15°C$, whereas Ose (1993) and Kristjánsson (1994) assumed a lower limit of $-40°C$. Part of the reason for this discrepancy is the limited number of observations that are available, and the somewhat conflicting nature of these. (See section 3a.)

While it may be possible to capture the time-averaged properties of the clouds using interpolation in temperature, it is not possible to simulate the evolution of cloud systems in a realistic way. In real mixed-phase clouds, condensate forms initially mainly as liquid water, because of the relative scarcity of ice-forming nuclei, but the ice crystals then grow by vapor deposition at the expense of the liquid-water droplets, because the saturation vapor pressure is lower with respect to ice than with respect to liquid water (often referred to as the Bergeron–Findeisen mechanism). It is also desirable that the treatment should account for the observed fact that, at a given temperature, deep clouds are more likely to be glaciated than thin clouds (Ryan 1996), since the lower levels of deep clouds are seeded by ice falling from above. This *seeder–feeder mechanism* is thought to be responsible for most of the precipitation produced by midlatitude stratiform clouds (e.g., Rutledge and Hobbs 1983). A specific problem with the interpolation-based approach is that ice that falls into a subfreezing layer may be forced to melt, in order to achieve the prescribed liquid fraction that is assumed to exist at that temperature (Rotstayn 1997). This is obviously unrealistic.

The developers of some recent cloud schemes have allowed the microphysics to determine the liquid fraction in mixed-phase clouds, rather than simply prescribing this fraction as a function of temperature. Lohmann and Roeckner (1996) included physically based treatments of condensational growth of water droplets and depositional growth of ice crystals, but did not show results that allowed comparison of their modeled liquid fractions with observations. Del Genio et al. (1996) did not actually allow ice and liquid water to coexist in a grid box, but instead specified the phase as either liquid or ice by first calculating a temperature-based liquid fraction and, then, comparing this interpolated value with a random number. They then included a simple parameterization of the Bergeron–Findeisen mechanism, which allowed the lower layers of multilayer clouds to be seeded by ice falling from above. They compared their liquid fractions with aircraft observations taken over the continental former Soviet Union (Feigelson 1978) and found good agreement for grid points over land. Ghan et al. (1997) applied a somewhat simplified version of the Colorado State University Regional Atmospheric Modeling Systems (RAMS) microphysical scheme to a GCM, and even included a prognostic variable for the ice crystal number concentration. They also compared their results with the Soviet aircraft data and concluded that too few of the clouds in the model contained supercooled liquid water. Rotstayn (1997) tried a simple treatment of the Bergeron–Findeisen mechanism that was driven primarily by the relative difference between the saturation vapor pressures over ice and liquid water at a given temperature. He compared his modeled liquid fractions with measurements made in frontal and other stratiform clouds by the Meteorological Research Flight of the UKMO and found that the results from the model agreed quite well with the observations. However, there are some conceptual problems with his approach, as was noted in the paper. In particular, a weakness of the scheme is that it allows ice to form in the absence of liquid water even at temperatures close to 0°C, whereas in reality the formation of ice at these temperatures normally requires liquid water to form first.

This paper describes an improved scheme, which addresses the conceptual problems with the method of Rotstayn (1997), and also gives results that look realistic when compared to observations. The scheme is physically based but is not expensive in terms of computer time. The central part of the scheme is a physically based calculation of the growth of cloud ice crystals by vapor deposition at the expense of coexisting cloud liquid water. The details of the scheme are given in section 2. The variation with temperature of the modeled liquid water fractions is compared with observations in section 3, which also includes the results of sensitivity tests. The performance of the scheme in a limited-area model simulation of a frontal cloud system is evaluated in section 4. Section 5 contains discussion, and section 6 contains a summary. The appendix contains a list of symbols. Système Internationale (SI) units are used throughout the paper, except where indicated otherwise.

2. Description of the parameterization

a. Models and cloud scheme

The parameterization of the liquid fraction has been implemented in the Commonwealth Scientific and Industrial Research Organisation (CSIRO) GCM and in the CSIRO Division of Atmospheric Research Limited

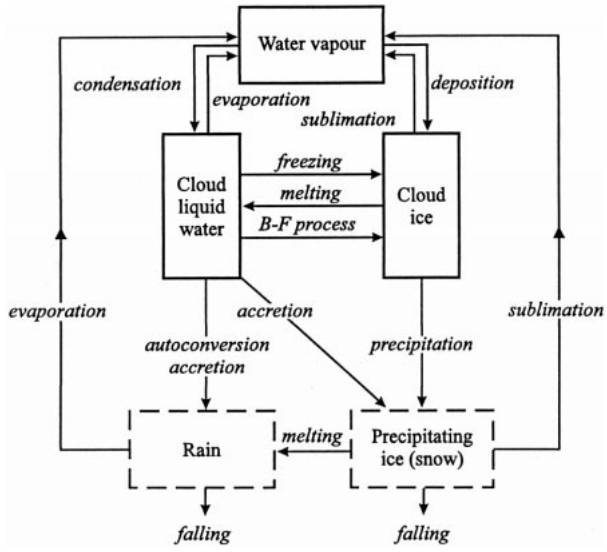

FIG. 1. Schematic overview of the microphysical processes treated by the prognostic cloud scheme. *B–F process* refers to the Bergeron–Findeisen process discussed in the text.

Area Model (DARLAM) as a modification of the prognostic cloud scheme described by Rotstayn (1997). The version of the CSIRO GCM used here is a low-resolution (spectral R21) version, with 18 vertical sigma levels (Rotstayn 1997). At this resolution, the required time step is 24 min, but because of the leapfrog scheme used by the model, the time step effectively ''seen'' by the physics is 48 min. DARLAM is a semi-Lagrangian model and has been described by McGregor et al. (1993). The simulations reported in section 4 were performed with horizontal resolution of 30 km, and 18 vertical sigma levels. The time step used was 10 min.

The cloud scheme incorporates prognostic variables for cloud liquid water and cloud ice, whereas rain and precipitating ice (snow) are diagnostic quantities that are not carried forward in time. Figure 1 shows a schematic overview of the microphysical processes that are treated. The scheme includes physically based treatments of precipitation processes, and interactive calculation of cloud radiative properties. The cloud radiative properties are calculated based on the cloud liquid water and cloud ice contents that are generated by the cloud scheme. Also included in the scheme are vertical turbulent mixing and semi-Lagrangian advection of cloud liquid water and cloud ice. A diagnostic treatment of convective cloudiness, similar to that described by Slingo (1987), has been retained at present. This study deals only with the treatment of stratiform clouds.

Stratiform cloud formation and dissipation are calculated using an assumed triangular probability distribution function (PDF) for the mixing ratio of total (vapor plus cloud) water in a grid box. Cloud water then forms in the part of each grid box in which the total-water mixing ratio exceeds the saturated value. This scheme (Smith 1990; Rotstayn 1997, 1998) retains the use of a prescribed critical relative humidity that controls the onset of cloud formation; it is this critical relative humidity that defines the standard deviation of the PDF for the moisture distribution within each grid box. In the CSIRO GCM, the critical relative humidity is set to 0.85 over oceans, and 0.75 over land. The cloud fraction C and the cloud-water mixing ratio q_c depend on (i) the difference between the total water mixing ratio and the saturated value in a grid box, and (ii) the critical relative humidity. The calculation of cloud formation and dissipation corresponds to the four conversion terms shown toward the top of Fig. 1. One benefit of including a treatment of fractional cloudiness is that the microphysical processes can be formulated in terms of cloud-averaged, rather than grid-box-mean, quantities. Cloud-averaged quantities (such as cloud-water mixing ratios) are more closely related to what would be observed in real clouds.

Once the cloud-water mixing ratio is calculated, a method is required to partition this into cloud liquid water (q_l) and cloud ice (q_i). At temperatures colder than -40°C, cloud liquid water freezes instantaneously to form cloud ice. At temperatures warmer than 0°C, cloud ice melts instantaneously to form cloud liquid water. These are the freezing and melting terms shown in the center of Fig. 1. There is another term that converts cloud liquid water to cloud ice, namely the Bergeron–Findeisen mechanism of ice crystal growth by vapor diffusion at the expense of liquid water. In essence, this is the topic of the present paper. Although there is an intermediate stage in which the water exists in the gas phase, the process is equivalent to the freezing of cloud liquid water to form cloud ice. The liquid fraction is defined as

$$f_l = \frac{q_l}{q_l + q_i}. \tag{1}$$

The liquid fraction can be used to also define a liquid-water cloud fraction $C_l = f_l C$, and an ice-cloud fraction $C_i = (1 - f_l)C$.

Once the mixing ratios of cloud liquid water and cloud ice are calculated, the scheme calculates the depletion of cloud liquid water and cloud ice by precipitation. These processes are shown in the lower half of Fig. 1. Cloud liquid water is depleted by autoconversion (i.e., collision and coalescence of cloud droplets), collection of cloud liquid water by rain, and accretion of cloud liquid water by snow. The last term amounts to a treatment of the seeder–feeder mechanism mentioned in the introduction. It enhances the development of precipitation in the lower layers of deep clouds, which are represented as multilayer clouds in the model (Rotstayn 1997). Precipitation of cloud ice is calculated using an observationally based fall speed, on the assumption that ice particles grow quickly by diffusion to sufficient size to acquire appreciable fall speeds. In the absence of separate prognostic variables for snow and cloud ice,

snow that falls into a layer during a time step is added to the cloud ice field in that layer. (This approximation is discussed in section 5.) Evaporation of rain and sublimation of snow are included, using parameterizations that account for the different properties of raindrops and snow particles. Snow melts instantaneously to form rain when it enters a layer that is warmer than 2°C.

Clouds are assumed to be randomly overlapped in the vertical, which is consistent with the assumption used in the model's radiation scheme. The vertical overlap assumption can have a marked effect on the parameterized microphysical processes (Jakob and Klein 1999). Randomly overlapped clouds give higher rates of evaporation of precipitation, but lower rates of accretion of cloud liquid water by precipitation, than would be obtained using a maximum overlap assumption.

b. Overview of the method

In the CSIRO GCM, a statistical condensation scheme is used for the calculation of stratiform cloud formation and dissipation, but the method is not limited to being used with this type of condensation scheme. In the scheme, ice and liquid water are allowed to coexist at temperatures between −40° and 0°C, so an assumption must be made about the phase of the condensate. When cloud formation occurs, it is assumed that all new condensate forms as liquid water. This is physically reasonable, because ice formation at temperatures above −40°C usually requires liquid water to form first. When cloud dissipation occurs, it is assumed that any cloud liquid water that is present evaporates first, followed by any cloud ice that is present. Again, this is physically reasonable, because the saturation vapor pressure is lower with respect to ice than with respect to liquid water. The latter assumption has less effect on the model than the former assumption, because cloud dissipation occurs at only about 20% of the points in the model that contain stratiform cloud.

The condensation scheme also requires the specification of a suitable value for the saturation vapor pressure, and there is some doubt regarding how to make this choice in the temperature range in which liquid water and ice are allowed to coexist in a grid box. For example, Fowler et al. (1996) used a weighted average of the values with respect to ice and liquid water, with the weights specified as a linear function of temperature between 0° and −20°C. In contrast, Lohmann and Roeckner (1996) allowed mixed-phase clouds to exist between 0° and −35°C, and assumed saturation with respect to ice when ice was already present, or saturation with respect to liquid water otherwise.

In the present scheme, when $-40°C < T < 0°C$, saturation with respect to liquid water is assumed initially in the condensation calculation. Note that this implies that the air in the cloudy part of the grid box is saturated with respect to liquid water and is consistent with the previous assumption that condensate forms initially as liquid water. However, if the subsequent calculation of the growth of cloud ice at the expense of liquid water shows that the cloud has completely glaciated, the condensation scheme is rerun with the assumption of ice saturation. This is a simplification, because in real ice clouds the air would generally be somewhere in between water and ice saturation, but it is consistent with the assumption made for ice clouds at temperatures below −40°C, and also in many other models. We are currently working on a scheme that aims to determine the saturation level in ice clouds from physical principles.

Next, the growth of cloud ice crystals by vapor deposition at the expense of coexisting cloud liquid water is calculated. Different versions of this calculation have been derived, based on different assumptions about

- the spatial relationship of the coexisting cloud ice and liquid water,
- the specification of the ice crystal number concentration, and
- the ice-crystal habit.

When liquid water and ice coexist in a grid box (i.e., if $f_l > 0$), an assumption must be made regarding their spatial relationship. The two simplest assumptions are *horizontally adjacent* and *uniformly mixed*. In the former case, the cloud is assumed to consist of two horizontally adjacent components, one consisting solely of liquid water and the other consisting solely of ice. In the latter case, the liquid water and ice are assumed to be uniformly mixed throughout the cloud.

The calculation of vapor deposition on cloud ice takes slightly different forms, depending on which of these assumptions is used. In the horizontally adjacent case, small ice crystals each of initial mass M_{i0} are assumed to form in the liquid-water part of the cloud, and then grow by vapor deposition. In the uniformly mixed case, it is the preexisting ice crystals that grow by vapor deposition throughout the entire cloud. (See Fig. 2.)

The vapor deposition parameterization is derived in section 2c for the assumptions of spherical ice particles and horizontally adjacent liquid water and ice. A key component of the scheme is the specification of the ice crystal number concentration; this is discussed in section 2d. The treatment of different ice crystal habits (hexagonal plates and columns) is considered in section 2e. Use of the uniformly mixed assumption requires only a small change to the scheme and is discussed in section 2f.

c. Growth of cloud ice by vapor deposition

The growth rate of an ice crystal of mass M_i is given by (Rogers and Yau 1988; Pruppacher and Klett 1997)

$$\frac{dM_i}{dt} = \frac{4\pi\mathcal{C}(S_i - 1)}{A'' + B''}, \tag{2}$$

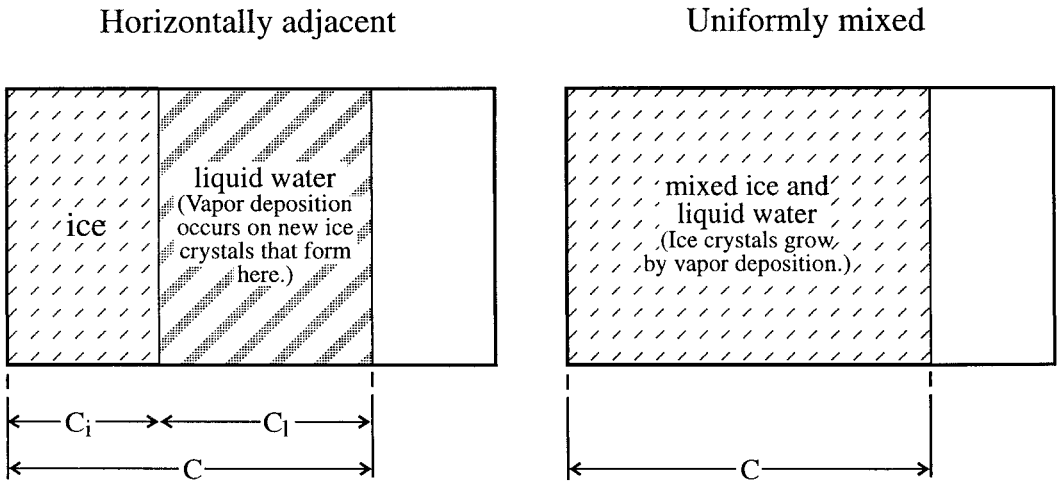

FIG. 2. Schematic illustration of the spatial relationship of cloud ice and cloud liquid water when using the horizontally adjacent and uniformly mixed assumptions.

where $\mathcal{C}$ is the capacitance, $S_i = e/e_{si}$ is the saturation ratio, and

$$A'' = \frac{L_s}{K_a T}\left(\frac{L_s}{R_v T} - 1\right) \tag{3}$$

and $B'' = R_v T/\chi e_{si}$ are terms representing heat conduction and vapor diffusion, respectively. Here χ is the diffusivity of water vapor in air, which varies inversely with pressure as $\chi = 2.21/p$ in SI units. If the ice crystal number concentration is N_i and the ice crystals at a grid point are monodispersed, with all particles having mass M_i, then the local (as distinct from grid-box mean) value of the cloud-ice mixing ratio is $\tilde{q}_i = M_i N_i/\rho$. If the air is at water saturation, so that $S_i - 1 = (e_{sl} - e_{si})/e_{si}$, then the rate of change of $\tilde{q}_i$ is

$$\frac{d\tilde{q}_i}{dt} = \frac{N_i}{\rho}\frac{4\pi\mathcal{C}(e_{sl} - e_{si})}{(A'' + B'')e_{si}}. \tag{4}$$

For the idealized case of spherical ice crystals of diameter D_i and constant density ρ_i, the capacitance is $\mathcal{C} = D_i/2$, where $D_i = (6M_i/\pi\rho_i)^{1/3}$. Elimination of $\mathcal{C}$ from (4) then gives

$$\frac{d\tilde{q}_i}{dt} = \left(\frac{N_i}{\rho}\right)^{2/3}\frac{7.8\tilde{q}_i^{1/3}(e_{sl} - e_{si})}{\rho_i^{1/3}(A'' + B'')e_{si}}. \tag{5}$$

During the course of a time step, the temperature will change by only a fraction of a degree due to the release of latent heat of fusion, so temperature-dependent quantities in (5) may be treated as constants for practical purposes. However, $\tilde{q}_i$ may increase by orders of magnitude during a time step, so it is beneficial to treat $\tilde{q}_i$ as a variable and to integrate (5) analytically with respect to time, in order to reduce the magnitude of time-truncation errors. This yields

$$\tilde{q}_i(t) = \left(\frac{2}{3}c_{vd}^s t + \tilde{q}_{i0}^{2/3}\right)^{3/2}, \tag{6}$$

where

$$c_{vd}^s = 7.8\frac{(N_i/\rho)^{2/3}(e_{sl} - e_{si})}{\rho_i^{1/3}(A'' + B'')e_{si}} \tag{7}$$

and $\tilde{q}_{i0} = M_{i0}N_i/\rho$ is the assumed initial mixing ratio of cloud ice in the part of the cloud that contains supercooled liquid water. Following Rutledge and Hobbs (1983), it is assumed that $M_{i0} = 10^{-12}$ kg; it is shown in section 3c that there is little sensitivity to the value of M_{i0}. Ryan et al. (1976) found ice crystal densities to lie in the range 400–900 kg m^{-3}, so $\rho_i = 700$ kg m^{-3} can be taken as a typical value.

It is assumed that as the ice grows by vapor deposition, liquid water evaporates to keep the air at saturation with respect to liquid water. Thus, ice grows at the expense of liquid water, so the net process can be represented as *freezing*. The growth of cloud ice is limited by the available amount of liquid water. If the model time step is Δt, and the growth of cloud ice is assumed to occur only in the fraction C_l of the grid box that contains liquid water, then the total amount of cloud liquid water that is converted to ice in a time step Δt is given by

$$\Delta q_i = \min\left[q_l, C_l\left(\frac{2}{3}c_{vd}^s\Delta t + \tilde{q}_{i0}^{2/3}\right)^{3/2}\right]. \tag{8}$$

A temperature increase (of magnitude $L_f\Delta q_i$), due to the release of latent heat of fusion, is applied instantaneously to the grid-box-mean temperature field.

d. Specification of the ice crystal number concentration

The ice crystal number concentration N_i in (7) is specified following Meyers et al. (1992) as a function of ice

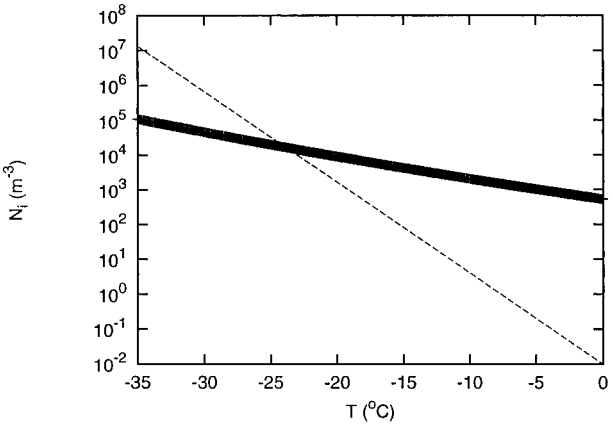

FIG. 3. Variation with temperature of the ice crystal number concentration given by (9) (thick line) and (10) (dashed line).

supersaturation. Assuming that the air is at water saturation, the parameterization can be written as

$$N_i = 10^3 \exp[12.96(e_{sl} - e_{si})/e_{si} - 0.639]. \quad (9)$$

This parameterization is based on continuous-flow diffusion-chamber measurements of ice nuclei, which suggest that the ice supersaturation is the primary quantity that controls the concentration of ice nuclei that are activated by deposition nucleation or condensation–freezing nucleation. Meyers et al. (1992) pointed out that it is difficult in nature to separate the processes of ice crystal nucleation via the deposition and condensation–freezing modes and suggested describing them by a single mode. They found that (9) gave good agreement with measured concentrations of ice nuclei and generated realistic distributions of ice crystal number concentration in mesoscale model simulations of a wintertime orographic precipitation event over the Sierras in central California.

Some earlier microphysical schemes (e.g., Rutledge and Hobbs 1983) have used a relation first suggested by Fletcher (1962) to parameterize the ice crystal number concentration as a function of temperature. Fletcher's relation is

$$N_i = 10^{-2} \exp[\beta(T_0 - T)], \quad (10)$$

where T_0 is the freezing point of water and typically $\beta = 0.6\ \mathrm{K}^{-1}$. Figure 3 shows the variation with temperature of N_i as predicted by (9) and by (10). Since e_{sl} and e_{si} are functions of temperature, (9) implies a variation of N_i with temperature. Equation (10) gives much lower ice crystal concentrations at warmer temperatures, but larger concentrations below about −25°C. It is now thought that the Fletcher relation (10) strongly underestimates N_i at warmer temperatures and overestimates N_i below about −25°C (Bower et al. 1996). The effect of using (10) instead of (9) to parameterize N_i is considered in section 3c.

Note that modified versions of (9) and (10) that introduce a height-dependent correction have been proposed by Sassen (1992) and DeMott et al. (1994), respectively. However, there is conflicting observational evidence regarding whether concentrations of ice nuclei really decrease with height as suggested by these modified parameterizations (Pruppacher and Klett 1997).

e. Different ice crystal habits

Ice crystal habits in real clouds are a complex function of temperature and ice supersaturation; see for example Rogers and Yau (1988, Fig. 9.6) for a summary of laboratory results, or Platt (1997) for a discussion of measurements taken in real clouds. It is beyond the scope of a scheme designed for use in large-scale models to treat this degree of complexity in a realistic way, but it is still of interest to test the sensitivity of the scheme to the ice crystal habit.

If the ice is assumed to exist in the form of hexagonal platelike crystals, the derivation of the vapor deposition equation is similar to the derivation for spherical crystals, but with different forms for the capacitance and the mass–diameter relationship. Hexagonal plates can be modeled as circular disks of diameter D_i, for which $\mathcal{C} = D_i/\pi$ (Rogers and Yau 1988; Pruppacher and Klett 1997). Following Rutledge and Hobbs (1983), the diameter of a hexagonal plate can be related to its mass as $D_i = 16.3M_i^{1/2}$. It follows that

$$\Delta q_i = \min\left[q_l, C_l\left(\frac{1}{2}c_{vd}^p \Delta t + \tilde{q}_{i0}^{1/2}\right)^2\right], \quad (11)$$

where

$$c_{vd}^p = 65.2\frac{N_i^{1/2}(e_{sl} - e_{si})}{\rho^{1/2}(A'' + B'')e_{si}}. \quad (12)$$

Note that this assumption gives the computationally cheapest form of the scheme, because (11) and (12) can be coded using integer-valued exponents only.

The equation for the rate of vapor deposition on columnar crystals is again derived in a similar manner, but with a different form for the capacitance and for the mass–length relationship. Columnar crystals may be modeled as prolate spheroids of semimajor and semiminor axes a and b, for which

$$\mathcal{C} = \frac{A}{\ln[(a + A)/b]}, \quad (13)$$

where $A = (a^2 - b^2)^{1/2}$ (Rogers and Yau 1988; Pruppacher and Klett 1997). According to Heymsfield (1972), for a small columnar crystal of length up to 0.3 mm, $b = 0.5a$, so the capacitance reduces to

$$\mathcal{C} = \frac{\sqrt{3}L_i}{4\ln(2 + \sqrt{3})}, \quad (14)$$

where $L_i = 2a$ is the longest dimension (length) of the crystal. From Platt (1997), the length (in SI units) of a column of mass M_i is $L_i = 0.203M_i^{0.339}$. It follows that

$$\Delta q_i = \min[q_l, C_l(0.661 c_{vd}^c \Delta t + \tilde{q}_{i0}^{0.661})^{1.51}], \quad (15)$$

where $c_{vd}^c = 0.839(N_i/\rho)^{0.661}(e_{sl} - e_{si})/[(A'' + B'')e_{si}]$. Note that the general form of the vapor-deposition equation is

$$\Delta q_i = \min\{q_l, C_l[(1 - \alpha)c_{vd}^{s,p,c}\Delta t + \tilde{q}_{i0}^{1-\alpha}]^{1/(1-\alpha)}\}, \quad (16)$$

where the rate constant $c_{vd}^{s,p,c}$ is different for each crystal habit as indicated above, and $\alpha = \frac{1}{3}$ for spheres, ½ for plates, or 0.339 for columns.

f. Uniformly mixed clouds

For the case of liquid water and ice that are uniformly mixed throughout the cloud, the form of the vapor deposition equation is almost unchanged, except that

- the deposition process occurs in the whole cloud, so that C_l is replaced by C;
- the initial cloud-ice mixing ratio is set equal to the preexisting in-cloud value when ice already exists; and
- the preexisting cloud-ice mixing ratio must be subtracted from the final value to obtain the correct expression for Δq_i.

Thus, for the case of spherical ice crystals, (8) is replaced by

$$\Delta q_i = \min\left[q_l, C\left(\frac{2}{3}c_{vd}^s\Delta t + \tilde{q}_{i0}^{2/3}\right)^{3/2} - q_i\right], \quad (17)$$

where now $\tilde{q}_{i0} = \max(M_{i0}N_i/\rho, q_i/C)$ and q_i is the cloud-ice mixing ratio in the grid box prior to the vapor deposition calculation (but after the condensation scheme is called). The rate constant c_{vd}^s is again given by (7). This form of the parameterization is expected to give faster rates of conversion of liquid water to ice, because when there are preexisting ice crystals they will in general be larger than the very small crystals that are assumed to form initially when the horizontally adjacent form of the parameterization is used. [Equation (4) shows that the conversion rate depends on the capacitance, which increases linearly with the crystal diameter.]

3. Variation with temperature of the liquid fraction

a. Observations

Figure 4 shows measurements of f_l taken in frontal and a limited number of other stratiform clouds by the UKMO Meteorological Research Flight. The observations show low liquid fractions over a fairly wide temperature range, as was noted by Bower et al. (1996). Note that this figure differs somewhat from the figure shown by Bower et al., which included frontal clouds only. Comparison of these two figures shows that the shallower nonfrontal stratiform clouds (such as stratocumulus) typically have somewhat higher liquid fractions than the deep frontal clouds.

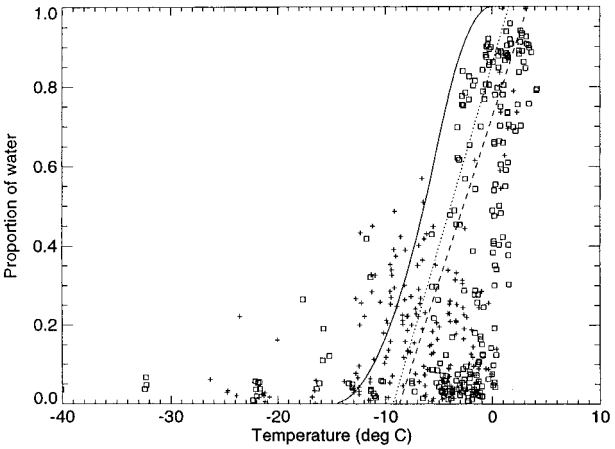

FIG. 4. Variation with temperature of the liquid fraction from aircraft observations, obtained as described by Bower et al. (1996). Crosses represent observations in continental clouds and squares represent observations in maritime clouds. The solid curve represents a parameterization that has been used in the UKMO GCM. The dashed and dotted lines represent lines of best fit derived for maritime and continental clouds separately by Bower et al. (1996). Reproduced from Ryan (1996).

The finding of low liquid fractions in deep frontal clouds was also mentioned by Ryan (1996) in a review of observations of precipitating layer clouds. He argued that at temperatures below −15°C the amount of liquid water is low away from the strong updrafts in regions of embedded convection. This suggests that the supercooled liquid water at these temperatures in frontal cloud systems should be generated principally by the convective parameterizations in models, rather than by the stratiform cloud parameterizations. It also suggests that there is a problem with trying to validate stratiform cloud parameterizations using the climatology of cloud phase as a function of temperature shown by Feigelson (1978), because Feigelson showed data for all clouds combined. This climatology, based on extensive aircraft observations taken over the former Soviet Union, suggests that there is plenty of liquid water in clouds at temperatures below −15°C, but it is difficult to say to what extent this occurs in convective clouds.

Several of the observational studies reviewed by Ryan (1996) found evidence of liquid water at temperatures down to −30°C or even lower. This generally occurred in shallower clouds, rather than in the deep frontal systems. So the dataset from Bower et al. (1996) may underestimate the incidence of supercooled liquid water in a global sense, because it contains relatively few observations from nonfrontal stratiform clouds. Further evidence that this may be the case comes from satellite microwave measurements, which find liquid water down to −25° or −30°C (Curry et al. 1990). However, we are not aware of any such measurements that have been

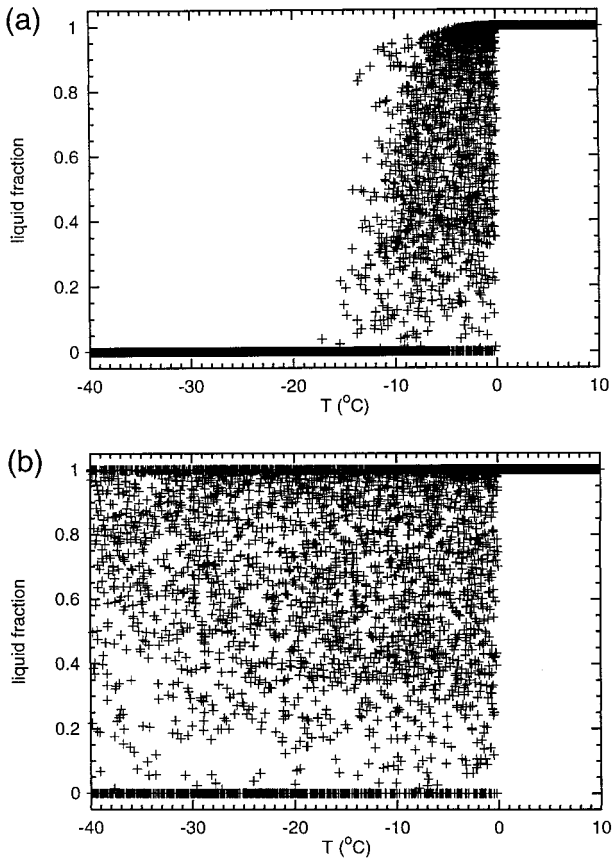

FIG. 5. Variation with temperature of the liquid fraction predicted by the model (a) using the standard version of the scheme, and (b) with the vapor-deposition calculation turned off.

published in the form of a climatology that is suitable for model validation.

In summary then, we choose to compare the results from the model with the data from Bower et al. (1996), essentially because of a lack of clearly better alternatives. However, the reservations expressed above should be borne in mind while reading the following sections.

b. Standard version of the scheme

Figure 5a shows the variation with temperature of the liquid fractions generated by the *standard version* of the scheme, as described in sections 2c and 2d. The values of f_l shown were obtained from a single time step of a run performed for conditions corresponding to the beginning of July using the scheme in the CSIRO GCM. (Values obtained from other time steps are very similar to those shown.) Before saving the liquid fractions, the model was run for 24 h from an initial condition obtained from another run in which the liquid fractions were calculated as described by Rotstayn (1997). Each liquid fraction was calculated from (1) using mixing ratios that were taken as the average of the values obtained before and after the calculation of precipitation. Thus,

$$q_l = \frac{q_l^{(1)} + q_l^{(2)}}{2}, \tag{18}$$

where $q_l^{(1)}$ is the cloud liquid-water mixing ratio obtained after the calculation of cloud formation and the growth of ice crystals by vapor deposition, and $q_l^{(2)}$ is that obtained after the subsequent calculation of precipitation. The cloud-ice mixing ratios are averaged similarly. These are the same values of q_l and q_i that are used to calculate the cloud radiative properties. In nature the processes of condensation, growth of ice crystals, and precipitation formation are all happening continuously and in parallel, but in a large-scale model we are forced to use relatively large time steps. This averaging process at least seems to be preferable to using only the mixing ratios that are available, say, after the completion of the precipitation calculation, since these are generally smaller than those that exist before the precipitation calculation.

Figure 5a shows that at temperatures warmer than about -10°C, there are some clouds in the model that are mainly composed of either liquid water or ice, and many that are of mixed phase. Below about -10°C, the number of clouds that have large liquid fractions drops off rapidly with temperature, and below about -15°C almost all of the clouds are completely glaciated.

The qualitative agreement between the modeled and observed fields is generally good, even though the number of observations is much smaller than the number of points saved from the model. The observations include a number of points at temperatures above freezing that have $f_l < 1$. This is because the melting of snow does not occur instantly once falling snow reaches the melting level. The model does not presently include a physically based calculation of the melting of snow or cloud ice. Falling snow melts instantly in the model when it reaches the 2°C level, and the cloud-formation scheme instantly melts cloud ice (i.e., it sets $f_l = 1$) when $T > 273.15$ K. Since the vapor deposition calculation is performed immediately after the cloud-formation scheme is called, the model results shown here do not admit the possibility of $f_l < 1$ when $T > 273.15$ K.

For comparison, Fig. 5b shows the liquid fractions obtained from the same time step if the vapor deposition calculation is turned off. Clearly, the liquid fractions at lower temperatures are too high in this case. The difference between these liquid fractions and those shown in Fig. 5a gives an indication of the effect of the parameterized vapor deposition process in converting liquid water to ice.

The parameterized rate of conversion of liquid water to ice, obtained from the model as $\Delta q_i/(C_l \Delta t)$, is plotted in Fig. 6 and is strongly correlated with temperature. This is because the term $(e_{sl} - e_{si})/e_{si}$ in (9) is a function of temperature only, and because the thermodynamic

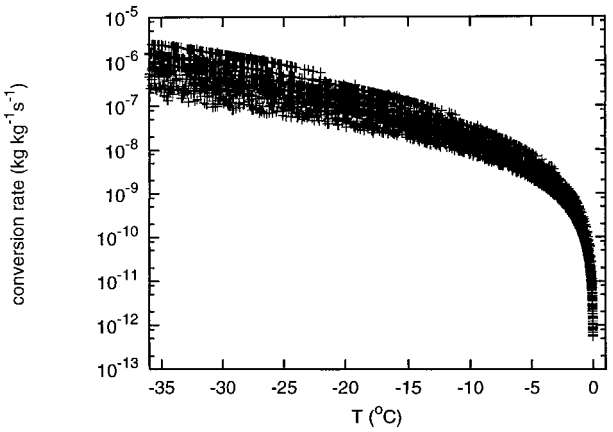

FIG. 6. Variation with temperature of the the parameterized rate of conversion of liquid water to ice in the model.

terms A'' and B'' are also mainly functions of temperature. The scatter in Fig. 6 is due to the appearance of p in the expression for B'' and the appearance of ρ in (7).

c. Sensitivity tests

The following sensitivity tests were performed using the CSIRO GCM as described above. Each test represents a single change with respect to the standard version of the scheme that was used in section 3b.

1) Effect of ice crystal number concentration

Figure 7a shows the liquid fractions obtained when Fletcher's (1962) relation (10) is used instead of (9) to parameterize the ice crystal number concentration. Because (10) gives lower values of N_i at higher temperatures, it results in lower rates of conversion of liquid water to ice. Comparison of the liquid fractions in Fig. 7a with the observed values in Fig. 4 shows that, based on this dataset, Fletcher's relation gives liquid fractions that are too large. A scheme similar to that described in this paper, but using (10) instead of (9), was discussed briefly by Rotstayn (1997). It was rejected because the ice crystal number concentrations given by Fletcher's relation are thought to be too small at warmer temperatures (Bower et al. 1996), and because the resulting liquid fractions produced by the model appeared to be too large.

One of the reviewers of this paper asked whether the scheme is capable of generating supercooled liquid water at relatively low temperatures, for example as might be observed in air that is lacking in ice nuclei. To show how the scheme would respond to much lower concentrations of ice nuclei, we have repeated the standard run, but with the ice crystal number concentration given by (9) reduced by a factor of 100. The results in Fig. 7b show that, when N_i is reduced by a factor of 100, the

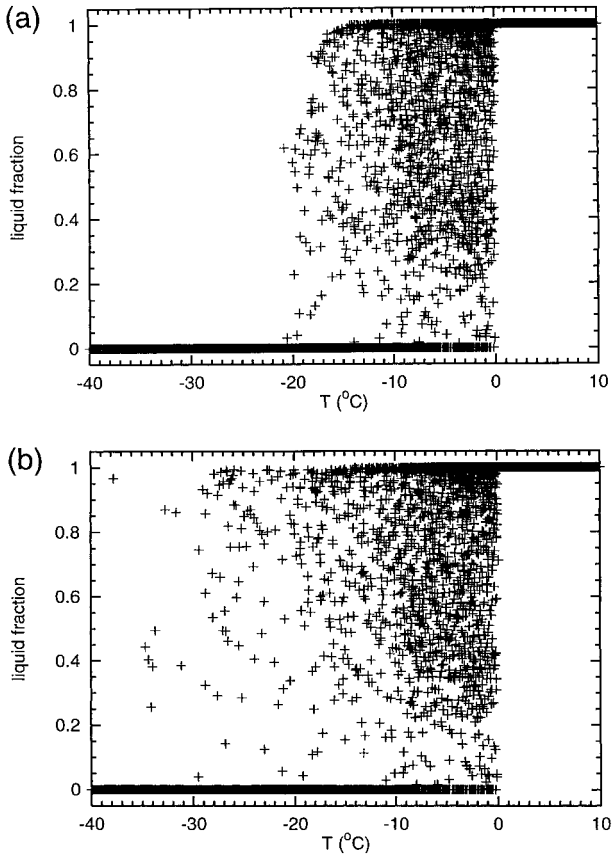

FIG. 7. Variation with temperature of the liquid fraction predicted by the scheme when (a) the ice crystal number concentration is obtained from Fletcher's relation (10), or (b) the ice crystal number concentration is reduced by a factor of 100 relative to that given by (9).

scheme generates considerably more supercooled liquid water, including at a few points with temperatures lower than −30°C. It should also be noted that the ability of the scheme to generate supercooled liquid water is somewhat limited at this coarse horizontal resolution, because the model can only produce weak updrafts. [See sensitivity test (5) below and section 5.]

2) Effect of initial size of ice crystals

The initial mass of each ice crystal, M_{i0}, is a tunable parameter, so it is of interest to evaluate the sensitivity of the modeled liquid fractions to the choice of M_{i0}. Two additional runs have been performed, one using a larger value $M_{i0} = 10^{-9}$ kg and one using a smaller value $M_{i0} = 10^{-15}$ kg. The liquid fractions from the former run are shown in Fig. 8, which shows that the modeled liquid fractions are insensitive to an increase of M_{i0} (cf. Fig. 5a). A similar lack of sensitivity was found in the run with decreased M_{i0} (not shown).

The reason for the lack of sensitivity is that, even when the larger value $M_{i0} = 10^{-9}$ kg is used, the $\tilde{q}_{i0}^{2/3}$ term in (8) is typically more than an order of magnitude

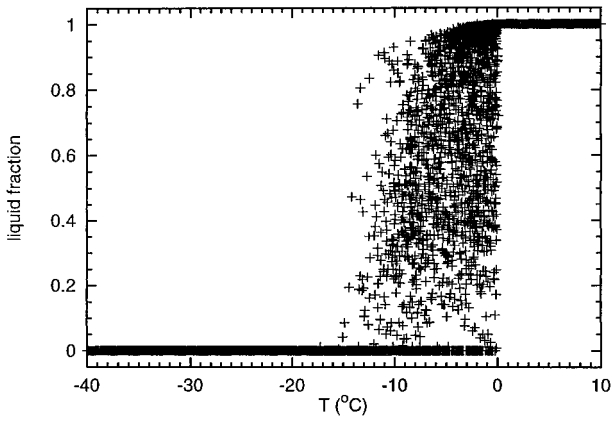

FIG. 8. Variation with temperature of the liquid fraction predicted by the scheme when the initial mass of the ice crystals is increased to 10^{-9} kg.

smaller than the $\frac{2}{3}c^{s}_{vd}\Delta t$ term. Increasing M_{i0} by another two orders of magnitude to 10^{-7} kg has a noticeable impact on the modeled liquid fractions, but such a value is not appropriate for the small ice crystals that are assumed to form initially.

3) EFFECT OF ICE CRYSTAL HABIT

As was mentioned earlier, ice crystals in real clouds are not generally spherical, so it is of interest to evaluate the sensitivity of the modeled liquid fractions to the assumed crystal habit. Results for hexagonal plates [Eq. (11)] and columns [Eq. (15)] are shown in Figs. 9a and 9b, respectively, and can be compared with the results for spheres shown in Fig. 5a. It can be seen that plates give lower liquid fractions overall than do spheres, while columns give slightly higher liquid fractions overall. This is because the plates have a higher growth rate than the spheres, whereas the columns have a slightly lower growth rate.

These differences can be understood in terms of the different expressions for the capacitance of each crystal type. Equation (4) shows that it is the capacitance that controls the different behavior of the different crystal types, because $\mathcal{C}$ is the only parameter in the equation that differs between the crystal types. To see the reason for the differences, it is necessary to write the capacitance in terms of the mass M_i of an individual ice crystal. For spheres of density 700 kg m^{-3}, $\mathcal{C} = 0.5D_i \approx 0.070M_i^{1/3}$. For plates, $\mathcal{C} \approx 0.32D_i \approx 5.2M_i^{1/2}$. For columns, $\mathcal{C} \approx 0.33D_i \approx 0.067M_i^{0.339}$. These expressions for the capacitance are plotted as a function of M_i in Fig. 10. At the start of each time step, when small crystals of mass 10^{-12} kg are initiated, the spherical crystals have a faster rate of growth than the columns or plates. However, as the crystals grow, the plates quickly overtake the spheres and columns. On the other hand, the columns have a slightly slower growth rate than the spheres throughout the relevant range of masses. (Results not shown indicate that crystal masses larger than 10^{-7} kg are not generated by the vapor-deposition calculation.) Thus, plates give the fastest growth rate, followed by spheres, closely followed by columns.

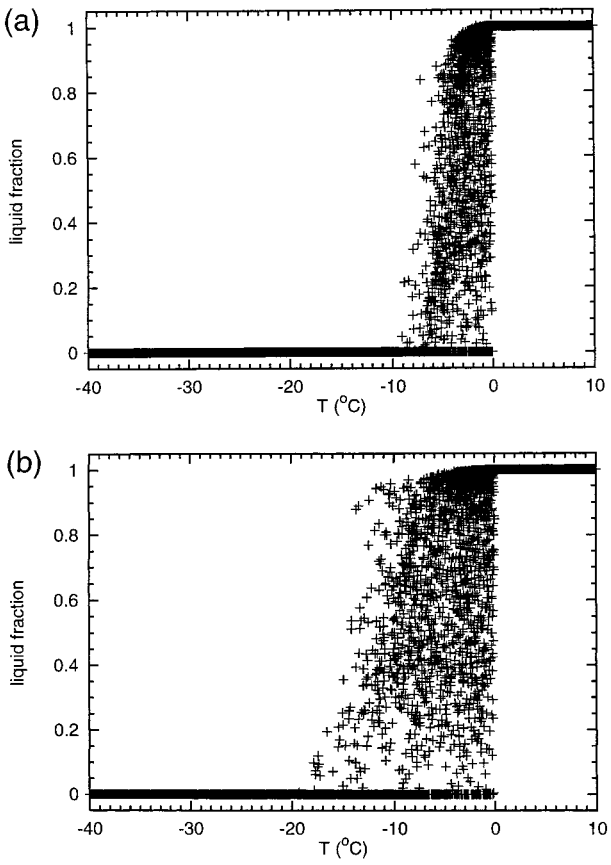

FIG. 9. Variation with temperature of the liquid fraction predicted by the scheme when the ice crystals are assumed to be in the form of (a) hexagonal plates or (b) columns, rather than constant-density spheres.

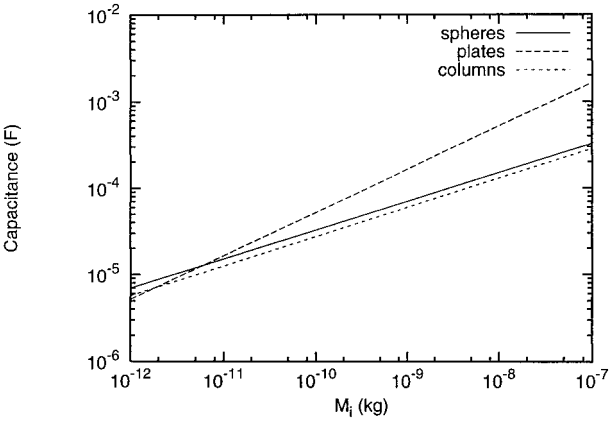

FIG. 10. Variation with mass of the capacitance of spherical, plate-like, and columnar ice crystals.

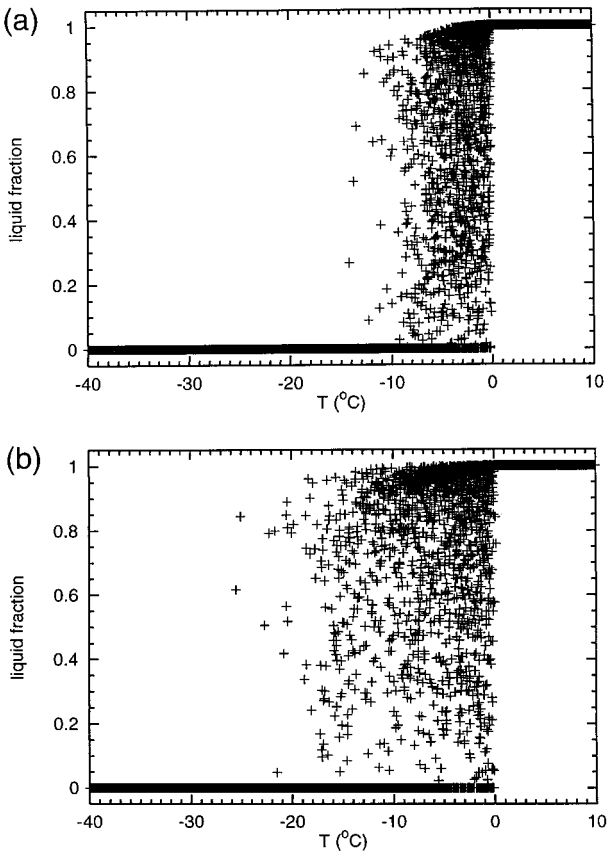

FIG. 11. Variation with temperature of the liquid fraction predicted by the scheme when (a) the cloud ice and cloud liquid water are assumed to be uniformly mixed, rather than horizontally adjacent, or (b) the horizontal resolution of the model is increased to spectral T63.

4) EFFECT OF ASSUMING UNIFORMLY MIXED CLOUDS

Figure 11a shows the variation with temperature of the liquid fractions generated by the model when the ice and liquid water are assumed to be uniformly mixed, rather than horizontally adjacent as in the standard version of the scheme. Comparison with Fig. 5a shows that there is some sensitivity to the assumed spatial relationship of the ice and liquid water. The liquid fractions obtained with the uniformly mixed assumption are overall somewhat lower than those obtained with the horizontally adjacent assumption. At temperatures colder than about -10°C, almost all of the clouds are completely glaciated.

The reason that there is not greater sensitivity is the relatively large leapfrog time step of 48 min used in the model. This gives the ice crystals plenty of time to grow to a reasonable size, even when the horizontally adjacent form of the parameterization is used. Greater sensitivity was obtained with the smaller time steps used in the limited-area simulations, as is discussed in the next section.

5) EFFECT OF HORIZONTAL RESOLUTION

It has been known for some time that cloud parameterizations often show sensitivity to horizontal resolution (e.g., Kiehl and Williamson 1991). In the case of the present scheme, it is to be expected that an increase of horizontal resolution will yield stronger updrafts and, will, hence, generate more liquid water. Figure 11b shows the liquid fractions generated by the model when using increased horizontal resolution (spectral T63). Data were saved only from every fifth longitude in the model, so that the number of points shown is comparable to that shown from the R21 model. As expected, the T63 model generates noticeably larger liquid fractions than the R21 model (cf. Fig. 5a). This is discussed further in section 5.

6) EFFECT OF SEEDER–FEEDER MECHANISM

As was discussed above, cloud layers that are seeded with ice that falls from above are expected to contain less supercooled liquid water than shallow clouds. Clouds in the former group are usually those that occur in the lower layers of multilayer clouds in the model, but could also be isolated cloud layers that have separate cloud layers overlying them, with clear air in between. In the latter case, the falling ice would evaporate in the clear layer(s), but that which does not evaporate could still affect the cloud layer below.

A convenient way to test whether this effect occurs in the model is to group the points according to whether or not there is a substantial flux of ice falling into the layer from above during the time step being considered. Figure 12 shows the liquid fractions generated at two subsets of the set of points shown in Fig. 5a. In Fig. 12a, points colder than 0°C for which there was no flux of ice entering the grid box from above are considered. In Fig. 12b, points colder than 0°C are shown for which the flux of ice entering the grid box during the time step exceeded 0.1 kg m^{-2}. (This threshold was chosen to make the number of points shown in Fig. 12b comparable to the number shown in Fig. 12a.) It is clear that the liquid fractions are smaller overall in Fig. 12b than in Fig. 12a. This shows that, qualitatively at least, the seeder–feeder effect is captured by the model. This behavior cannot be reproduced by a temperature-dependent parameterization of the liquid fraction.

4. Simulation of a frontal cloud system

In the previous section, we presented results obtained when the scheme was used in a low-resolution GCM. In this section, the scheme is used in simulations of a frontal system that have been performed with DARLAM, the CSIRO limited-area model.

The frontal system that is simulated here was observed in considerable detail during phase III of the Australian Cold Fronts Research Programme (CFRP;

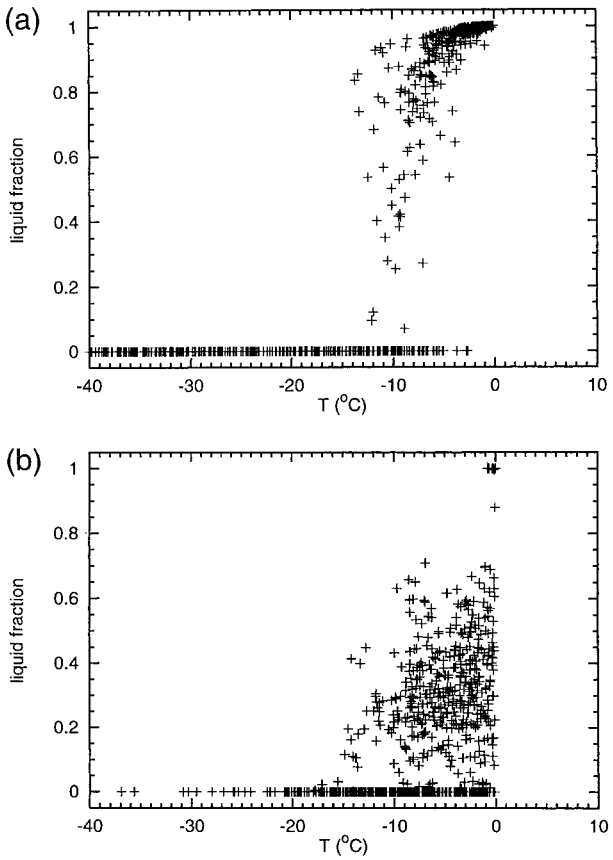

FIG. 12. As in Fig. 5a but showing only those points for which the flux of ice entering the grid box from above during the time step is (a) zero, or (b) greater than 0.1 kg m^{-2}.

Ryan et al. 1989). Between 17 and 19 November 1984, a cold front passed across the CFRP observing network. The front is considered to be typical of the summertime ''cool changes'' that are often experienced in southeastern Australia. The observations of this frontal system have been discussed by Ryan et al. (1989) and Katzfey and Ryan (1997). Although there are no microphysical observations from this case study, the microphysical characteristics of similar systems over southeastern Australia have been well documented (King 1982; Ryan et al. 1985). Deep clouds such as those observed during the passage of this front have been found to contain low fractions of liquid water, because these systems do not generally contain strong updrafts.

The DARLAM simulations are essentially the same as those described by Katzfey and Ryan (1997), except that Rotstayn's (1997) cloud and precipitation scheme is used instead of the scheme described by Katzfey and Ryan. As in that study, the model simulations were initialized with European Centre for Medium-Range Weather Forecasts analyses at 0000 UTC 17 November 1984 and were run for 48 h. The analyses were interpolated to the 30-km Lambert conformal grid used by the model. The simulations reported here used a time step of 10 min, rather than the 2-min time step that was found by Katzfey and Ryan to be necessary for the cloud microphysical scheme that they used. The case study has also been the subject of a recent model intercomparison that has been performed under the auspices of the Global Energy and Water Cycle Experiment (GEWEX) Cloud System Study (GCSS) (Ryan et al. 2000, manuscript submitted to *Mon. Wea. Rev.*). This intercomparison included DARLAM simulations very similar to those described here, but with the treatment of mixed-phase clouds that was described by Rotstayn (1997). Only results that are relevant to the calculation of the liquid fraction are presented here.

Figure 13a shows the simulated horizontal wind (vectors), the vertical velocity (contours), and the liquid fraction (shading) at the 0.62 sigma level at 0400 UTC 18 November, that is, 28 h into the model run. The temperature at this level is around −5°C (see Fig. 14). This simulation used the standard version of the scheme, except that the uniformly mixed assumption was used, rather than the horizontally adjacent assumption. The position of the front can be roughly inferred from that of the large cloud band, which is approximately coincident with the analysed front at that time as shown in Katzfey and Ryan (1997, Fig. 1a). The cloud band is associated with a large-scale updraft that is embedded in a northwesterly flow. There is a band of liquid water that forms on the western side of the cloud band as the northwesterly flow enters the cloudy region, but the eastern half of the cloud is mainly glaciated at this level. A small area of liquid water around $X = 35$, $Y = 40$ is associated with a weak updraft. The larger area of liquid water toward the southern end of the figure coincides with the position of the surface low (Katzfey and Ryan 1997).

Useful insights can be gained by comparison of these results with those obtained using a simpler scheme that specifies the liquid fraction as a function of temperature. Figure 13b shows the same fields from another simulation in which the liquid fraction was specified, based on observations by Bower et al. (1996), as

$$f_l = 0.0664(T - 273.15) + 0.621. \qquad (19)$$

This parameterization gives a liquid fraction of 0.621 at 0°C, decreasing linearly to zero at approximately −9.35°C. The results at this sigma level are very different from those obtained using the present scheme, with a liquid fraction of between 0.2 and 0.4 throughout most of the cloud band. Slightly larger liquid fractions are obtained at the northern end of the band, where the air is a little warmer.

Figure 14 shows the same results in the form of east–west cross sections taken through the vertical plane at $Y = 45$ in Fig. 13. The deep frontal cloud band can be clearly seen, and ahead of the front there is a layer of high cloud that is completely glaciated in both runs. In the temperature range between 0° and −20°C, the liquid

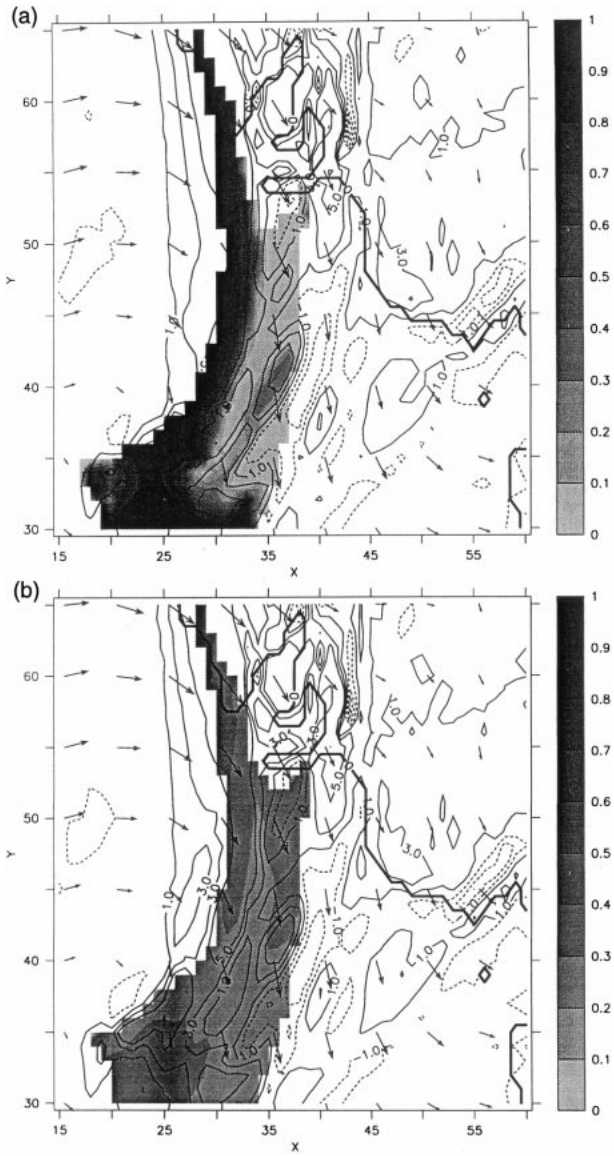

FIG. 13. Modeled liquid fractions (shading) and vertical velocity (contours) at the 0.62 sigma level, 28 h into the DARLAM simulation described in the text, obtained using (a) the uniformly mixed version of the scheme, and (b) the temperature-dependent parameterization (19). The vertical velocities are in units of -0.1 Pa s^{-1} (i.e., upward motion is denoted by positive numbers). The direction of the horizontal wind is shown by vectors at every fifth grid point. The thick lines show the position of the Australian coastline. The axes show the indices of the horizontal coordinates of the model's Lambert conformal grid.

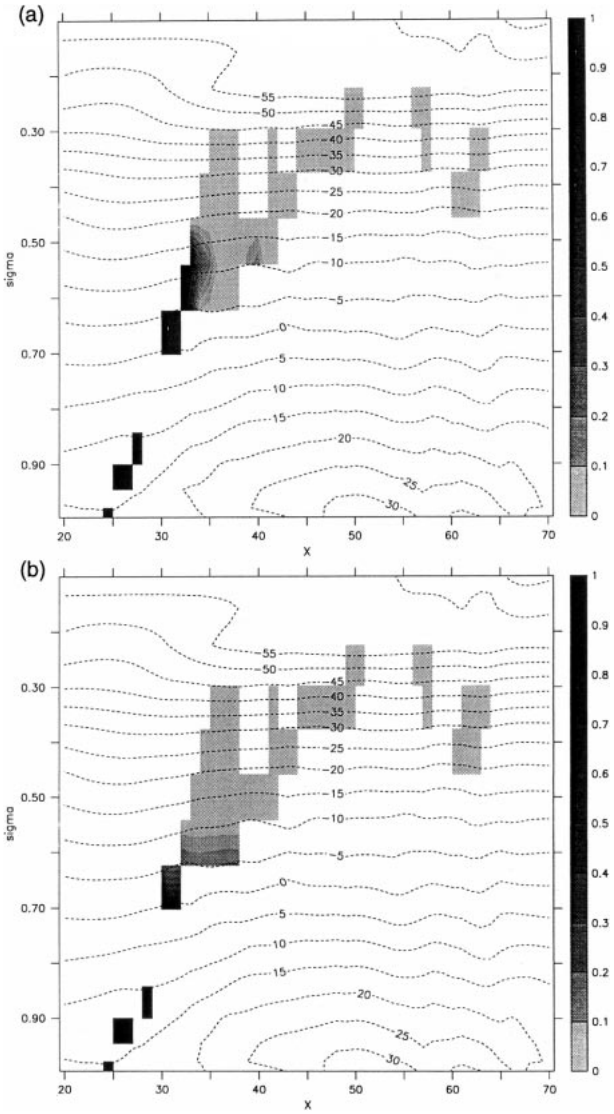

FIG. 14. East–west cross sections, taken through the vertical plane at $Y = 45$ in Fig. 13, of the modeled liquid fractions (shaded), obtained using (a) the uniformly mixed version of the scheme, and (b) the temperature-dependent parameterization (19). The contours show the temperature in °C.

fractions from the two schemes are quite different. The results from the present scheme vary horizontally as well as vertically and clearly show an area of large liquid fraction in the western part of the cloud band. In contrast, the scheme of Bower et al. gives the expected smooth variation with temperature, which varies mainly in the vertical.

We are not able to say with confidence whether or not the present scheme gives results that are more realistic than those obtained using the Bower et al. scheme, because there are no microphysical observations from this case study. In very broad terms, the results from both schemes are considered to be reasonable, based on the microphysical observations of similar cloud systems mentioned previously. However, the result given by the present scheme that the mature parts of the cloud are mostly glaciated down to the melting level is thought to be realistic and cannot be reproduced by a temperature-dependent parameterization.

What happens when the horizontally adjacent assumption is used instead of the uniformly mixed assumption? The former assumption was the one that we

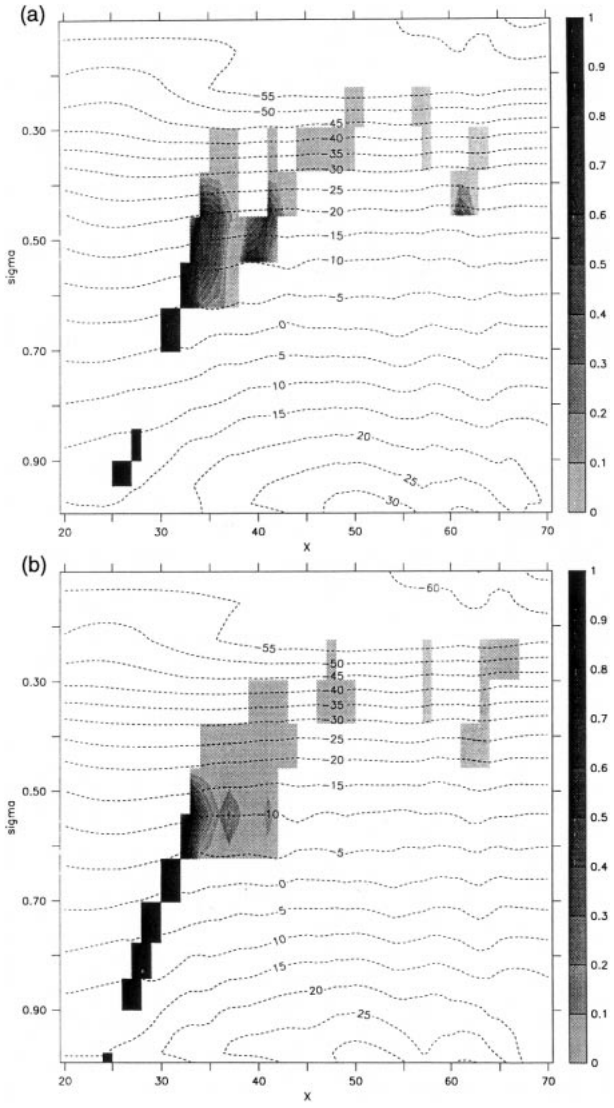

FIG. 15. As in Fig. 14a but using (a) the horizontally adjacent assumption instead of the uniformly mixed assumption, or (b) a time step of 1 min rather than 10 min.

tried initially in these simulations. However, as can be seen in Fig. 15a, this assumption allows liquid water to form almost up to the −30°C level. This is thought to be unrealistic for cloud systems of this type. Our first attempt to rectify the problem was to try a much smaller (1 min) time step, but this exacerbated the problem and allowed liquid water to form almost up to the −40°C level (not shown).

Why does the assumed spatial relationship of the cloud ice and liquid water have a larger impact in the DARLAM simulations than in the CSIRO GCM? The answer lies in the smaller 10-min time step used in DARLAM, compared to the 48-min leapfrog time step used in the GCM. Use of the horizontally adjacent assumption means that vapor deposition occurs on very small ice crystals that are initiated at every time step in the liquid-water part of the cloud. When a smaller time step is used, these ice crystals are initiated more frequently, and the vapor deposition process is not allowed to proceed far enough for these crystals to grow sufficiently large that the process becomes efficient. This is why the problem was exacerbated by the use of an even smaller time step. On the other hand, the uniformly mixed assumption allows vapor deposition to occur on preexisting ice crystals, and there is expected to be much less sensitivity to the time step when this version of the scheme is used.

Sensitivity to the time step is an undesirable feature of any parameterization, so we repeated the run with the uniformly mixed version using a 1-min time step, to check that this assumption really does give much less sensitivity to the time step. The resulting liquid fractions are shown in Fig. 15b, and are very similar to those in Fig. 14a, showing that the mixed-phase scheme is remarkably insensitive to the time step when the uniformly mixed assumption is used. There are some differences in the location of clouds below the melting level and also aloft. These are presumably related to changes in the modeled circulation, because the statistical condensation scheme does not involve a time step at all.

5. Discussion

The more realistic results and much lower sensitivity to the time step obtained in the limited-area simulations with the uniformly mixed assumption suggest that this is preferable to the horizontally adjacent assumption. However, this conclusion is based on only one case study, and should be tested in other cases. It should also be noted that these two assumptions represent opposite extremes, and it would be quite simple to introduce an intermediate assumption whereby a weighted mean of the two vapor-deposition calculations is used. This would require the introduction of a parameter to represent the fractions of ice and liquid water that are mixed together within the cloudy part of each grid box. It is less clear whether this parameter would have to be prescribed by tuning, or whether it is possible to specify it in a more physical way.

The sensitivity to horizontal resolution that was noted in section 3 is typical of existing cloud treatments in large-scale models (e.g., Kiehl and Williamson 1991). The ability of a model to resolve updrafts improves with increasing horizontal resolution, so it is to be expected that more liquid water will be generated by the condensation scheme in a higher-resolution model. As a result, there is likely to be more liquid water remaining after the ice crystals grow by the Bergeron–Findeisen process. But even a high-resolution GCM cannot resolve the updrafts that occur in real clouds. To some extent, this problem is addressed by the use of in-cloud values of cloud water contents, combined with the triangular PDF used by the con-

densation scheme. Reducing the critical relative humidity used by the scheme does increase the amount of liquid water that it generates (Rotstayn 1999). This is consistent with the notion that a lower-resolution model should use lower values of the critical relative humidity, because a reduction of the latter is physically equivalent to an increase in the assumed amount of subgrid variability of the moisture distribution. However, tuning this parameter remains a very crude approach. It should also be noted that while all of the microphysical parameterizations in the present scheme are formulated in terms of cloud-averaged quantities, it may eventually prove necessary to integrate the budget equations over subgrid distributions of the relevant variables. It is hoped that a concrete outcome of GCSS will be improved methods to parameterize the subgrid variability of key quantities such as vertical velocity. This should allow a more rigorous approach to the problem of subgrid variability.

The marked difference between the results obtained in cloud layers that were seeded by ice falling from above and cloud layers that were not (Fig. 12) is encouraging and suggests that the scheme is indeed able to distinguish between the properties of deep and shallow clouds, at least in a qualitative sense. This result depends on other components of the cloud scheme that allow ice entering from above to affect a cloud layer. In the present scheme, these are the inclusion of a term representing accretion of cloud liquid water by snow, and the fact that snow that falls into a layer during a time step is added to the cloud ice field in that layer. If the cloud layers did not interact, there would be no mechanism in the model that could give the behavior shown in Fig. 12.

One of the more uncertain aspects of the scheme is the parameterization of the ice crystal number concentration. Good results were obtained using a formulation due to Meyers et al. (1992) that depends on the ice supersaturation. This is a convenient form for use in the present scheme, because the assumption that the cloudy air is at water saturation when liquid water is present means that the ice supersaturation is easily calculated. However, it is clear that this approach represents a simplification of the microphysics of real mixed-phase clouds. A more comprehensive parameterization would be required to capture the differences between clouds that form in air that is abundant in or depleted of ice nuclei. One specific consequence of using this parameterization of the ice crystal number concentration is that the scheme does not contain any mechanism that will generate larger liquid-water fractions in continental clouds compared to maritime clouds, as suggested by the observations in Fig. 4. According to Rangno and Hobbs (1994), larger ice crystal concentrations are associated with the broader droplet size distributions that are typically found in maritime clouds, but the mechanism is uncertain. A more comprehensive approach might require the inclusion of a prognostic variable for ice crystal number concentration (e.g., Cotton et al. 1986; Ghan et al. 1997). However, this would result in a substantial increase in computational complexity, while retaining a substantial degree of uncertainty due to the currently incomplete understanding of the processes involved.

Measured ice crystal concentrations can be much higher than the values given by the parameterization of Meyers et al. (1992) in clouds in which ice-multiplication processes are active (Bower et al. 1996). However, ice-multiplication processes are, for the most part, thought to be associated with ice particles of precipitable size. For example, the comparatively well studied Hallett–Mossop effect (Hallett and Mossop 1974) is associated with the splintering of graupel particles that have grown by riming (accretion) of liquid water. The neglect of ice-multiplication processes in the present scheme can be justified because the scheme is treating the growth of cloud ice crystals rather than the growth of *precipitating* ice particles. The growth by vapor deposition of precipitating ice particles (loosely, snow) can be treated in an analogous way to the treatment of the sublimation of snow; the only difference between the two parameterizations is that the air is supersaturated for the case of vapor deposition, and subsaturated for the case of sublimation (Rotstayn 1997). A comprehensive microphysical scheme should ideally treat the growth of precipitating ice particles by both vapor deposition and accretion of cloud liquid water. Rotstayn (1997) included the latter process, but did not include the former one, because it would have been inconsistent with the assumption made in that version of the scheme that the air inside mixed-phase clouds is saturated with respect to ice.

The distinction made in the previous paragraph between cloud-ice and precipitating-ice particles raises some thorny issues regarding cloud parameterization. The first is that the present scheme, in common with most other schemes used in large-scale models, has only one prognostic variable to represent all forms of atmospheric ice. This simplification necessitates the use of one of two approximations. Some schemes use an approximation whereby snow is assumed to fall through the atmosphere in a model time step. However, this approximation is difficult to justify based on the length of typical model time steps (say, half an hour), and typical fall speeds of snow (less than 1 m s^{-1}). Also, Rotstayn (1997) found that the ''fall through'' approximation had a rather large impact on the results in tests performed with a GCM. In the present scheme, an alternative approximation is made whereby snow that falls into a model layer is added to the cloud ice field in that layer. While this may be preferable to the fall through approximation, it means that the distinction between the small cloud ice particles and the larger precipitating particles is lost. This suggests that it may be necessary to include a separate prognostic variable for snow as distinct from cloud ice (e.g., Fowler et al. 1996). How-

ever, the observations shown in Fig. 4 include the effects of *all* ice particles (small and large) that were measured in the clouds under consideration. So, the use of separate variables to represent cloud ice and snow might require that special care be taken when comparing models with observations.

It should also be noted that while the scheme described in this paper makes the simplifying assumption that the ice particles are monodispersed, ice particles in real clouds are not monodispersed. There is evidence that the larger particles approximately follow an exponential (Marshall–Palmer) size distribution, whereas the smaller ones approximately follow a power-law (Heymsfield–Platt) size distribution (Platt 1997). A more complete parameterization would account for these differing size distributions, although it remains to be seen whether taking this into account would have an impact that is any larger than the uncertainties that have already been discussed.

The scheme has been tested in one case study and gave results that are thought to be realistic. The selected case study was of a frontal system that did not include strong updrafts, and the scheme gave the expected result that the mature parts of the cloud system were mostly glaciated down to the melting level. Tests on more strongly forced systems should also be performed, as systems with stronger updrafts are expected to contain larger amounts of supercooled liquid water. Tests based on other case studies should also shed further light on the relative merits of the different assumptions that have been tried, in particular the choice of ice-crystal habit and the assumed spatial relationship of the ice and liquid water. Ideally, these case studies should include high quality microphysical observations, so that the scheme can be more thoroughly validated. The results obtained in any case study may be model dependent, so it would be beneficial to evaluate the performance of the scheme in a variety of models also.

We did not find that the method used to calculate the liquid fraction had a substantial impact on the timing of the front in the limited-area simulations. Katzfey and Ryan (1997) found that there was a significant dynamical impact due to the evaporative cooling in the subcloud layer, but the smaller release of latent heat of fusion in the cloud layer appears to be less important in this case. However, this should be investigated in further case studies, as the dynamical impact of the treatment of mixed-phase clouds could be significant in other situations. Since the present scheme is expected to generate more supercooled liquid water in systems that have strong updrafts, the modeled liquid fractions in such systems will probably differ more strongly from those that would be obtained using the temperature-dependent parameterization of Bower et al. (1996).

Tests of this scheme or similar schemes in convectively active situations will raise questions about the parameterization of the microphysics of convective clouds. This problem did not arise in the case study investigated here, because the model did not generate convective rainfall in the region occupied by the cloud band in Fig. 13. (Some convective activity was generated when the front passed over land.) Since pockets of supercooled water at temperatures lower than -15°C in frontal cloud systems are likely to be associated with regions of embedded convection (Ryan 1996), it can be argued that these should be treated in a model as part of the *convective* parameterization. However, present convection schemes that are used in large-scale models include only the most rudimentary treatments of microphysics; this is another topic for future research. Even if the liquid fraction is to be parameterized as a function of temperature, these observations suggest that models should distinguish between the properties of stratiform and convective clouds.

In this study we have not evaluated the effect of the new mixed-phase cloud treatment on the climate of the CSIRO GCM. One reason for this is that the liquid fractions generated by the new scheme are, in a gross sense, rather similar to those generated by our earlier scheme (Rotstayn 1997). We could have chosen to compare our scheme with one of the temperature-dependent parameterizations that have been used in other GCMs, but then the effect of the change on standard cloud-related fields such as liquid water path or shortwave cloud forcing would be a strong function of the choice of this parameterization. Probably more interesting would be to consider the effect of the scheme on statistics of variability, for example as revealed by eddy kinetic energies or transient eddy heat transports. We would prefer to look at these issues in the context of a higher-resolution model, such as the T63 version of the CSIRO GCM, which is currently being finalized. We have therefore chosen to defer such investigations until a later study.

6. Summary

We have described a scheme that can be used to calculate the liquid fraction in mixed-phase stratiform clouds in large-scale atmospheric models. The scheme is physically based but is not computationally expensive. The advantage of the approach, compared to the simple temperature-based parameterizations that have been widely used, is that it makes it possible to simulate the life cycles of mixed-phase clouds and the differences between deep and shallow clouds. The scheme has been presented here in association with a statistically based condensation scheme, but it is suitable for use with other prognostic cloud schemes also. The main prerequisite before the scheme can be used in another model is that the model must include separate prognostic variables for cloud liquid water and cloud ice. However, to obtain realistic results it may also be necessary for the model to include processes that allow cloud layers to be seeded by ice that falls from above.

The key features of the scheme are as follows.

- The assumption that all condensate within the temperature range −40° to 0°C forms initially as liquid water.
- An assumption about the spatial relationship of coexisting liquid water and ice, for example, horizontally adjacent or uniformly mixed within the cloudy part of a grid box. (See sections 2b and 2f.)
- A physically based calculation of the growth of ice crystals by vapor deposition at the expense of coexisting liquid water (the Bergeron–Findeisen mechanism). In the horizontally adjacent case, small ice crystals are assumed to form in the liquid-water part of the cloud and then grow by vapor deposition. In the uniformly mixed case, it is the preexisting ice crystals that grow by vapor deposition throughout the entire cloud. Versions of this calculation have been derived for three different ice crystal habits, namely spheres, hexagonal plates, and columns. (See sections 2c and 2e.)
- A parameterization of the ice crystal number concentration that is needed for the vapor-deposition calculation. The scheme was tested using Fletcher's (1962) temperature-dependent expression for the ice crystal number concentration, and using a parameterization due to Meyers et al. (1992) that depends on the ice supersaturation. (See section 2d.)

The variation with temperature of the modeled liquid fractions was found to be broadly realistic compared to the observations of Bower et al. (1996) when the scheme was used in a R21 version of the CSIRO GCM, provided that the supersaturation-dependent parameterization of the ice crystal number concentration was used. When Fletcher's expression was used, the scheme generated liquid fractions that appeared to be too large. There was also considerable sensitivity to the ice crystal habit and some sensitivity to the assumed spatial relationship of the liquid water and ice, but it is difficult to say which of these assumptions gave the best results. There was very little sensitivity to the assumed initial mass of the small ice crystals that form in the liquid-water part of each cloud when the horizontally adjacent assumption is used. There was a marked sensitivity to horizontal resolution, with the scheme generating larger liquid fractions when it was tried in a T63 version of the GCM. This shows that the liquid fractions generated with the GCM are constrained by its limited ability to resolve updrafts. A further test showed that the liquid fractions are lower in cloud layers that are seeded from above by falling ice, than in layers that are not seeded in this way. This shows that, at least qualitatively, the scheme is able to capture the different properties of deep and shallow clouds.

The scheme was also tested in simulations of a frontal system over southeastern Australia. These were performed at 30-km resolution using DARLAM, the CSIRO limited-area model. For comparison, simulations were also performed in which the liquid fraction was specified as a linear function of temperature following Bower et al. (1996). The present scheme generated substantial amounts of supercooled liquid water in the updraft where cloud formed initially in the northwesterly flow, but mature parts of the cloud were mostly glaciated down to the melting level. This behavior, which is considered to be realistic based on observations of similar cloud systems, was not captured by the temperature-dependent parameterization. In contrast to the results obtained with the GCM, the variation with temperature of the liquid fraction showed a rather strong sensitivity to the assumed spatial relationship of the liquid water and ice. This was because of the smaller time step used in DARLAM, which meant that, when the horizontally adjacent assumption was used, the ice crystals that were initiated at each time step did not have time to grow sufficiently large for the vapor-deposition process to become efficient. The results obtained using the uniformly mixed assumption are considered to be more realistic than those obtained using the horizontally adjacent assumption, but further tests based on other case studies are warranted. Another argument in favor of the uniformly mixed assumption is that the results obtained in DARLAM with this assumption were much less sensitive to the time step than when the horizontally adjacent assumption was used.

In conclusion, we suggest that the following combination of assumptions provides a version of the scheme that is suitable for further testing in other models and in other case studies. There was little sensitivity to the choice of the initial ice crystal mass, so there is no reason to vary this parameter from the value of 10^{-12} kg suggested by Rutledge and Hobbs (1983). There is a clear indication that it is preferable to parameterize the ice crystal number concentration following Meyers et al. (1992), rather than using Fletcher's (1962) expression. The results obtained in the limited-area simulations suggest that the assumption of uniformly mixed cloud liquid water and cloud ice is preferable to the assumption of horizontally adjacent cloud liquid water and cloud ice. Regarding the choice of ice crystal habit, it should be noted that similar results were obtained for spherical and columnar crystals. Since no single choice of ice crystal habit is correct, the simplest assumption of spherical crystals provides a good starting point for further tests.

Acknowledgments. This work contributes to the CSIRO Climate Change Research Program and is partly funded through Australia's National Greenhouse Research Program. The authors thank Jorgen Jensen, Debbie Abbs, and two anonymous reviewers for their comments on the manuscript, and Sarah Moss of the UKMO, who provided Fig. 4 in electronic form.

APPENDIX
List of Symbols

Symbol	Description	Value	Units
A''	Term representing heat conduction in the deposition equation		m s kg^{-1}
B''	Term representing vapor diffusion in the depostion equation		m s kg^{-1}
a	Semimajor axis of a prolate spheroid		m
b	Semiminor axis of a prolate spheroid		m
C	Stratiform cloud fraction		
$\mathcal{C}$	Capacitance of an ice particle		F
C_i	Stratiform ice-cloud fraction		
C_l	Stratiform liquid-water cloud fraction		
c^c_{vd}	Rate constant for vapor deposition on columnar ice crystals		s^{-1}
c^p_{vd}	Rate constant for vapor deposition on platelike ice crystals		s^{-1}
c^s_{vd}	Rate constant for vapor deposition on spherical ice crystals		s^{-1}
D_i	Diameter of a spherical or platelike ice crystal		m
e	Water vapor pressure		Pa
e_{si}	Saturation vapor pressure with respect to ice		Pa
e_{sl}	Saturation vapor pressure with respect to liquid water		Pa
f_l	Liquid fraction in mixed-phase clouds		
K_a	Thermal conductivity of air	2.40×10^{-2}	J m^{-1} s^{-1} K^{-1}
L_f	Latent heat of fusion of water	3.35×10^{5}	J kg^{-1}
L_i	Length of a columnar ice crystal		m
L_s	Latent heat of sublimation of water	2.834×10^{6}	J kg^{-1}
M_i	Mass of an ice crystal		kg
M_{i0}	Initial mass of an ice crystal	10^{-12}	kg
N_i	Ice-crystal number concentration		m^{-3}
p	Air pressure		Pa
q_c	Grid-box-mean cloud-water mixing ratio		kg kg^{-1}
q_i	Grid-box-mean cloud-ice mixing ratio		kg kg^{-1}
$\tilde{q}_i$	Local value of cloud-ice mixing ratio		kg kg^{-1}
$\tilde{q}_{i0}$	Initial local value of cloud-ice mixing ratio		kg kg^{-1}
q_l	Grid-box-mean of cloud-liquid-water mixing ratio		kg kg^{-1}
R_v	Specific gas constant for water vapor	461	J kg^{-1} K^{-1}
S_i	Saturation ratio with respect to ice		
T	Air temperature		K
T_0	Freezing point of water	273.15	K
t	Time		s
X	Index of x coordinate in limited-area model		
Y	Index of y coordinate in limited-area model		
β	Parameter in ice crystal concentration parameterization	0.6	K^{-1}
Δq_i	Change in q_i due to vapor deposition		kg kg^{-1}
Δt	Time step		s
ρ	Air density		kg m^{-3}
χ	Diffusivity of water vapor in air		m^2 s^{-1}

REFERENCES

Boucher, O., H. Le Treut, and M. B. Baker, 1995: Precipitation and radiation modelling in a GCM: Introduction of cloud microphysical processes. *J. Geophys. Res.,* **100,** 16 395–16 414.

Bower, K. N., S. J. Moss, D. W. Johnson, T. W. Choularton, J. Latham, P. R. A. Brown, A. M. Blyth, and J. Cardwell, 1996: A parametrization of the ice water content observed in frontal and convective clouds. *Quart. J. Roy. Meteor. Soc.,* **122,** 1815–1844.

Cotton, W. R., G. J. Tripoli, P. M. Rauber, and E. A. Mulvihill, 1986: Numerical simulation of the effects of varying ice crystal nucleation rates and aggregation processes on orographic snowfall. *J. Climate Appl. Meteor.,* **25,** 1658–1680.

Curry, J. A., C. D. Ardeel, and L. Tian, 1990: Liquid water content and precipitation characteristics of stratiform clouds as inferred from satellite microwave measurements. *J. Geophys. Res.,* **95,** 16 659–16 671.

Del Genio, A. D., M.-S. Yao, W. Kovari, and K. K.-W. Lo, 1996: A prognostic cloud water parameterization for climate models. *J. Climate,* **9,** 270–304.

DeMott, P. J., M. P. Meyers, and W. R. Cotton, 1994: Parameterization and impact of ice initiation processes relevant to numerical model simulations of cirrus clouds. *J. Atmos. Sci.,* **51,** 77–90.

Feigelson, E. M., 1978: Preliminary radiation model of a cloudy atmosphere. 1: Structure of clouds and solar radiation. *Beitr. Phys. Atmos.,* **51,** 203–229.

Fletcher, N. H., 1962: *The Physics of Rainclouds.* Cambridge University Press, 386 pp.

Fowler, L. D., D. A. Randall, and S. A. Rutledge, 1996: Liquid and ice cloud microphysics in the CSU general circulation model. Part I: Model description and simulated microphysical processes. *J. Climate,* **9,** 489–529.

Ghan, S. J., L. R. Leung, and Q. Hu, 1997: Application of cloud microphysics to NCAR community climate model. *J. Geophys. Res.,* **102,** 16 507–16 527.

Gregory, D., and D. Morris, 1996: The sensitivity of climate simulations to the specification of mixed phase clouds. *Climate Dyn.,* **12,** 641–651.

Hallett, J., and S. C. Mossop, 1974: Production of secondary ice particles during the riming process. *Nature,* **249,** 26–28.

Heymsfield, A. J., 1972: Ice crystal terminal velocities. *J. Atmos. Sci.,* **29,** 1348–1357.

Jakob, C., and S. A. Klein, 1999: The role of vertically varying cloud fraction in the parametrization of microphysical processes in the ECMWF model. *Quart. J. Roy. Meteor. Soc.,* **125,** 941–965.

Katzfey, J. J., and B. F. Ryan, 1997: Modification of the thermody-

namic structure of the lower troposphere by the evaporation of precipitation: A GEWEX cloud system study. *Mon. Wea. Rev.*, **125,** 1431–1446.
Kiehl, J. T., and D. L. Williamson, 1991: Dependence of cloud amount on horizontal resolution in the National Center for Atmospheric Research Community Climate Model. *J. Geophys. Res.,* **96,** 10 955–10 980.
King, W. D., 1982: Location and extent of supercooled water regions in deep stratiform cloud in western Victoria. *Aust. Meteor. Mag.*, **30,** 81–88.
Kristjánsson, J. E., 1994: Tests of a new cloud treatment in an atmospheric general circulation model. *Physica D,* **77,** 23–32.
Li, Z.-X., and H. Le Treut, 1992: Cloud-radiation feedbacks in a general circulation model and their dependence on cloud modelling assumptions. *Climate Dyn.,* **7,** 133–139.
Lohmann, U., and E. Roeckner, 1996: Design and performance of a new cloud microsphysics scheme developed for the ECHAM general circulation model. *Climate Dyn.,* **12,** 557–572.
McGregor, J. L., K. J. Walsh, and J. J. Katzfey, 1993: Nested modelling for regional climate studies. *Modelling Change in Environmental Systems,* A. J. Jakeman, M. B. Beck, and M. J. McAleer, Eds., Wiley, 367–386.
Meyers, M. P., P. J. DeMott, and W. R. Cotton, 1992: New primary ice-nucleation parameterization in an explicit cloud model. *J. Appl. Meteor.*, **31,** 708–721.
Ose, T., 1993: An examination of the effects of explicit cloud water in the UCLA GCM. *J. Meteor. Soc. Japan,* **71,** 93–109.
Platt, C. M. R., 1997: A parameterization of the visible extinction coefficient of ice clouds in terms of the ice/water content. *J. Atmos. Sci.,* **54,** 2083–2098.
Pruppacher, H. R., and J. D. Klett, 1997: *Microphysics of Clouds and Precipitation.* 2d ed. Kluwer, 974 pp.
Rangno, A. L., and P. V. Hobbs, 1994: Ice particle concentrations and precipitation development in small continental cumuliform clouds. *Quart. J. Roy. Meteor. Soc.,* **120,** 573–601.
Rasch, P. J., and J. E. Kristjánsson, 1998: A comparison of the CCM3 model climate using diagnosed and predicted condensate parameterizations. *J. Climate,* **11,** 1587–1614.
Raymond, D. J., and A. M. Blyth, 1992: Extension of the stochastic mixing model to cumulonimbus clouds. *J. Atmos. Sci.,* **49,** 1968–1983.
Rogers, R. R., and M. K. Yau, 1988: *A Short Course in Cloud Physics.* 3d ed. Pergamon Press, 293 pp.
Rotstayn, L. D., 1997: A physically based scheme for the treatment of stratiform clouds and precipitation in large-scale models. I: Description and evaluation of the microphysical processes. *Quart. J. Roy. Meteor. Soc.,* **123,** 1227–1282.
——, 1998: A physically based scheme for the treatment of stratiform clouds and precipitation in large-scale models. II: Comparison of modelled and observed climatological fields. *Quart. J. Roy. Meteor. Soc.,* **124,** 389–415.
——, 1999: Climate sensitivity of the CSIRO GCM: Effect of cloud modeling assumptions. *J. Climate,* **12,** 334–356.
Rutledge, S. A., and P. V. Hobbs, 1983: The mesoscale and microscale structure and organization of clouds and precipitation in midlatitude cyclones. VIII: A model for the ''seeder-feeder'' process in warm-frontal rainbands. *J. Atmos. Sci.,* **40,** 1185–1206.
Ryan, B. F., 1996: On the global variation of precipitating layer clouds. *Bull. Amer. Meteor. Soc.,* **77,** 53–70.
——, E. R. Wishart, and D. E. Shaw, 1976: The growth rates and densities of ice crystals between −3°C and −21°C. *J. Atmos. Sci.,* **33,** 842–850.
——, K. J. Wilson, J. R. Garratt, and R. K. Smith, 1985: Cold Fronts Research Programme: Progress, future plans, and research directions. *Bull. Amer. Meteor. Soc.,* **66,** 1116–1122.
——, ——, and E. J. Zipser, 1989: Modification of the thermodynamic structure of the lower troposphere by the evaporation of precipitation ahead of a cold front. *Mon. Wea. Rev.,* **117,** 138–153.
Sassen, K., 1992: Ice nuclei availability in the higher troposphere: Implications of a remote sensing cloud phase climatology. *Nucleation and Atmospheric Aerosols,* N. Fukuta and P. Wagner, Eds., Deepak Publishing, 287–290.
Slingo, J. M., 1987: The development and verification of a cloud prediction scheme for the ECMWF model. *Quart. J. Roy. Meteor. Soc.,* **113,** 899–927.
Smith, R. N. B., 1990: A scheme for predicting layer clouds and their water content in a general circulation model. *Quart. J. Roy. Meteor. Soc.,* **116,** 435–460.
WCRP, 1999: Report on the sixth session of the GEWEX Cloud System Study (GCSS) Science Panel. Informal Rep., WCRP, in press. [Available from WCRP/WMO, Case Postale 2300, CH-1211, Geneva 2, Switzerland.]